How to cite: Angew. Chem. Int. Ed. 2025, e202423281
doi.org/10.1002/anie.202423281

Operando Spectroscopy

Monitoring the Fate of Zn in the Cu/ZnO/ZrO_2 Catalyst During CO_2-to-Methanol Synthesis at High Conversions by *Operando* Spectroscopy

*Mariam L. Schulte, Vera Truttmann, Dmitry E. Doronkin, Lorena Baumgarten, Alexander Nicolai, Diego Alejandro Montalvo Beltran, Florian J. Summ, Christoph Kiener, Lucas Warmuth, Stephan Pitter, Erisa Saraçi, and Jan-Dierk Grunwaldt**

Abstract: In the frame of developing a sustainable chemical industry, heterogeneously catalyzed CO_2 hydrogenation to methanol has attracted considerable interest. However, the Cu–Zn based catalyst system employed in this process is very dynamic, especially in the presence of the products methanol and water. Deactivation needs to be prevented, but its origin and mechanism are hardly investigated at high conversion where product condensation is possible. Here, we report on the structural dynamics of a Cu/ZnO/ZrO_2 catalyst at 90 bar and 40 % CO_2 conversion (at equilibrium conditions), investigated in a dedicated metal-based spectroscopic cell specially fabricated using additive manufacturing. This particular reactor configuration aims to mimic the high CO_2 conversion part of the catalyst bed and can induce product condensation, which is monitored by *operando* X-ray absorption spectroscopy. While Cu remained mostly stable throughout the experiment, Zn underwent strong restructuring. The chosen reaction conditions, including the use of CO_2 as carbon source and *in situ* product condensation, were selected to provide insights under industrial conditions. This work is highlighting the importance of spectroscopic investigations at high conversion levels, offering insights into chemical transformations during deactivation, extending the concept of spatially resolved studies, and thus providing guidance for the design of more stable catalysts.

Introduction

Methanol (MeOH) synthesis, conventionally starting from synthesis gas (syngas, CO/H_2 and small amounts of CO_2) and employing the commonly used Cu/ZnO/Al_2O_3 (CZA) catalyst, has been vastly studied over the years.[1] Due to the promising approach to valorize CO_2 to produce valuable products like MeOH through hydrogenation using green hydrogen, the CO_2-to-MeOH reaction has gained increasing interest.[2] However, using CO_2 as feedstock imposes challenges due to the unfavorable thermodynamics[3] and, compared to CO-rich syngas, the higher amount of water formed leads to deactivation of the industrial CZA catalyst, e.g., by sintering and phase transformations.[4] The substitution of Al_2O_3 with ZrO_2 leads to improved performance and stability, making Cu/ZnO/ZrO_2 (CZZ) catalysts highly promising candidates for CO_2-to-MeOH synthesis.[2b,5] The promotional effect of ZrO_2 is vividly debated and can be attributed to its lower hydrophilicity,[2a,5a,6] enhanced CO_2 adsorption,[7] the formation of the Cu-ZrO_2 interface,[8] and the particularly selective ZnO-ZrO_2 interface.[9]

The ternary CZZ catalyst exhibits four different possible active interfaces: i) Cu-ZnO ii) Cu-ZrO_2 iii) ZnO-ZrO_2 and iv) ternary Cu-ZnO-ZrO_2. The Cu–Zn interface was widely studied for the CZA catalyst, yet the active state is still under debate.[1] Depending on the intensity of the reductive treatment (e.g., H_2 partial pressure), the formation of a Cu–Zn alloy or oxygen-deficient and defective ZnO, together with morphological changes of the Cu particles, has been observed.[10] Several studies have proposed the formation of a graphitic ZnO_{1-x} overlayer after reduction,[11] which can

[*] M. L. Schulte, Dr. V. Truttmann, Dr. D. E. Doronkin, L. Baumgarten, Dr. E. Saraçi, Prof. Dr. J.-D. Grunwaldt
Institute for Chemical Technology and Polymer Chemistry
Karlsruhe Institute of Technology
Engesserstr. 20, 76131 Karlsruhe, Germany
E-mail: grunwaldt@kit.edu

M. L. Schulte, Dr. D. E. Doronkin, L. Baumgarten, Dr. L. Warmuth, Dr. S. Pitter, Dr. E. Saraçi, Prof. Dr. J.-D. Grunwaldt
Institute of Catalysis Research and Technology
Karlsruhe Institute of Technology
Hermann-von-Helmholtz-Platz 1, 76344 Eggenstein-Leopoldshafen, Germany

A. Nicolai, D. A. Montalvo Beltran, F. J. Summ, C. Kiener
Foundational Technologies, Research & Predevelopment, Advanced Manufacturing & Circularity
Siemens AG
Otto-Hahn-Ring 6, 81739 Munich, Germany

partially convert to ZnO nano-islands under reaction conditions (e.g., syngas feed) that, under long time on stream, can be further transformed to a dense polycrystalline ZnO overlayer.[12] In addition to the Cu-ZnO interface and the Cu–Zn (surface) alloy, Zn-formate has also been proposed as an active species.[13] Besides the Cu-ZnO interface, interactions with ZrO_2 need to be considered for CZZ catalysts. The ZnO-ZrO_2 interface exhibits high selectivity towards methanol when applying ZnO-ZrO_2 catalysts in CO_2-to-MeOH synthesis.[9] When ZrO_2 is used as the support, the formed ZnO_x clusters or monodispersed Zn on the ZrO_2 surface were suggested as active sites.[14] By doping ZnO-ZrO_2 with Cu, a pronounced performance increase in comparison to pure ZnO-ZrO_2 was observed, attributed to the occurrence of low-nuclearity Cu–Zn clusters.[15]

In addition to the manifold proposed active interfaces, the nature of the active sites in Cu–Zn based catalysts is highly dynamic and susceptible to changes during reaction conditions.[1,10a] It is therefore crucial to investigate the catalyst structure during reaction, i. e., *operando*, under conditions as close to industrial ones as possible,[16] which, in the case of methanol synthesis from CO_2, translates to pressures between 50 and 100 bar, temperatures ranging from 200 to 250 °C, and water/MeOH formation.[17] One particularly suitable technique is X-ray absorption spectroscopy (XAS), which allows *operando* experiments at various pressures and temperatures. For the investigation of methanol synthesis by XAS, several spectroscopic cells and reactors have been applied in the past: While quartz capillary reactors generally allow experiments up to 20 bar, a specific *operando* cell developed in our group enabled investigations during methanol synthesis at 30 bar,[18] and experiments at 40 bar are possible with Be tube reactors.[19] Furthermore, Bansode et al.[20] could perform *operando* XAS measurements during CO_2 hydrogenation on a CZA catalyst at 200 bar and 260 °C in a capillary reactor system.

However, due to the small volume of the cells/reactors and the additional dilution required for spectroscopic investigations in transmission mode, *operando* XAS studies use only small amounts of catalysts. This results in differential conversions well below those used in industrial reactors, rendering the spectroscopic data less representative of the real-world scenarios. Although such studies have not been conducted during methanol synthesis, the importance of this aspect has been recently found to be critical, e.g. in ammonia decomposition/synthesis catalysts, where phase transformations have been observed at high ammonia concentrations.[21] Differential conditions, i. e., low conversion, are mostly chosen for kinetic investigations. Nevertheless, at high conversion, product concentrations are enhanced, resulting in considerable water formation during CO_2 hydrogenation, which is expected to be at the origin of catalyst degradation[4b] and was observed in spatially resolved studies during CO_2 methanation.[22] Therefore, experiments at high conversion levels are crucial, especially focusing on the end of a catalyst bed, where product concentration is the highest. Previous studies, mainly conducted at differential conversion, attributed deactivation to the loss of Cu-ZnO interfacial sites due to segregation, restructuring and crystallization.[4] A long-term stability study revealed sintering of Cu and restructuring of ZnO into an overlayer, as well as crystallization of ZnO as key descriptors of the deactivation.[11d] The study used a nearly identical CZZ catalyst to the one employed in this work. Furthermore, restructuring of the Cu–Zn interface induced by the presence of alcohol, e.g. MeOH, was proposed for a CZA catalyst,[23] further highlighting the need for investigations with substantial product amounts.

When considering MeOH synthesis at elevated pressures (above ca. 90 bar), condensation of liquid products can occur already at high temperatures (180 °C), which can be exploited to shift the equilibrium to the product side, as shown by different condensation reactor concepts.[24] At these pressures, condensed liquids lead to hydrothermal conditions in the reactor that can potentially severely alter the catalyst structure.[2b] In fact, *operando* studies of Cu–Zn based catalysts, focusing on detailed elucidation of the degradation process induced by condensed products with spectroscopic reactors that provide sufficient product quantities, are currently lacking.

Herein, we studied the catalyst structure of a highly active CZZ catalyst using a custom-made reactor for *operando* XAS during CO_2 hydrogenation to methanol up to a maximum CO_2 conversion (40 %) and elevated pressure (90 bar). The high conversion levels were achieved with the concept of an additively manufactured spectroscopic reactor, consisting of two consecutive catalyst beds in two independently controllable temperature zones. We investigated the structure of the lower catalyst bed with XAS, which mimics the conditions at the end of a fixed-bed reactor with elevated product concentrations. In the first catalyst bed, up to 2 g of catalyst enabled conversion up to the thermodynamically limited conversion level, whereas in the second part, 24 mg of CZZ catalyst diluted with SiO_2 was loaded to allow optimal conditions for spectroscopy. By inducing condensation of methanol and water in the catalyst bed *via* an enforced temperature drop, we further aimed to study deactivation phenomena in the catalyst structure. The overall goal was to gain insights into the restructuring of the catalyst at high product concentrations and thus to provide a basis for the knowledge-driven design of future methanol catalysts.

Results and Discussion

Additively Manufactured Spectroscopic Reactor for High Pressure Applications

High-pressure *operando* XAS experiments were performed in a novel spectroscopic reactor made by additive manufacturing (AM), as depicted in Figure 1 (details cf. ESI, section 1). To monitor the catalyst structure, X-ray transparent Beryllium windows with a field of view of 10×10 mm were used (Figure 1a). In the sectional view (Figure 1b), all features of the reactor are schematically displayed: The gas mixture enters the reactor through the inlet and passes

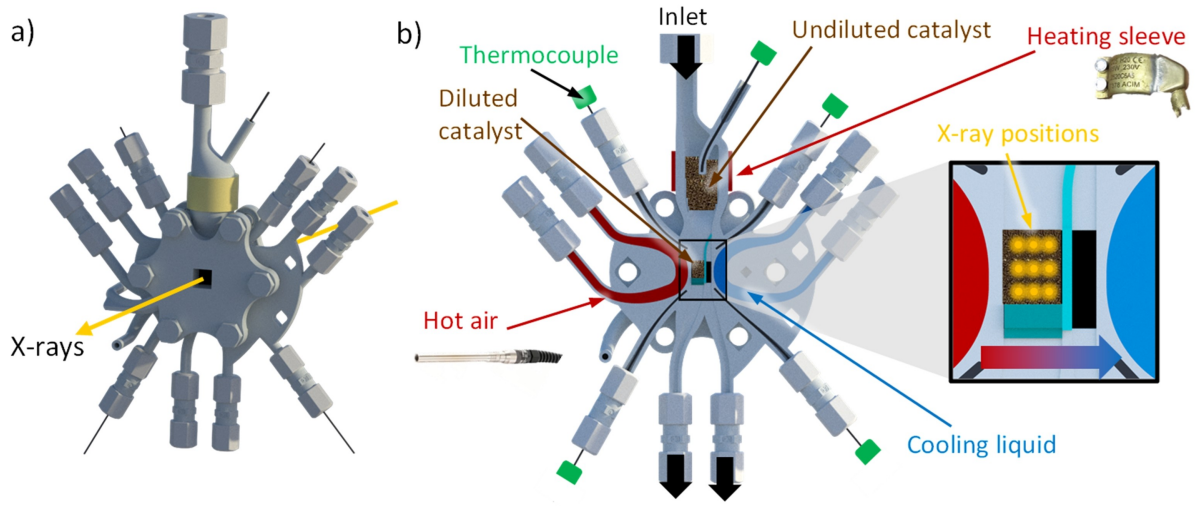

Figure 1. a) Front view of the additively manufactured reactor. b) Sectional view of the additively manufactured reactor with labeled components, including a zoomed view of catalyst bed area (inset) showing marked X-ray positions.

through the first catalyst bed, which is filled with undiluted catalyst positioned on top of a silicon carbide (SiC) bed to achieve high conversion and productivity. This upper part of the reactor ("upper zone") is heated using a heating sleeve, with temperature control provided *via* a thermocouple (type K) placed in a sheath inside the catalyst bed. The mixture of products and reactants then passes through the successive second catalyst bed with diluted catalyst located in the X-ray transparent part of the reactor ("window zone"). This zone is heated through a channel with flowing hot air from a gas blower (see Figure 1b). To introduce temperature gradients within this catalyst bed, a cooling liquid can be fed through a channel on the opposite site. With the two consecutive catalyst beds, one can mimic the conditions at the end of a fixed-bed reactor. In the first bed the temperature is kept at 235 °C to continuously produce significant amounts of products, which then pass through the second bed. The two independently controlled temperature zones enabled us to study potential catalyst deactivation by lowering the temperature in the second catalyst bed to induce condensation. We want to highlight that this multifunctionality was realized by the advanced AM of the cell applied here (details, cf. ESI). Moreover, the 10×10 mm window in the reactor allows spatially resolved measurements and a grid of 3×3 positions was scanned (Figure 1b, zoomed-in view, inset). The temperature of the window zone can be recorded at 4 positions with thermocouples placed close to the catalyst bed at the X-ray window (see ESI, Figure S6a for details). For sealing the X-ray windows, graphite and Be discs were used, similar to our previously developed cell,[18] allowing measurements up to 150 bar and 300 °C.

CO_2-to-Methanol Synthesis with High Conversion

The AM spectroscopic reactor was employed in the CO_2/H_2-to-MeOH reaction at 90 bar and at temperatures up to 250 °C using a new CZZ catalyst. CZZ production combines continuous nucleation under kinetically controlled conditions using a micromixer and subsequent batch aging of the initial precipitate in 4 L stirred tank reactors. A total of about 0.4 kg CZZ catalyst was produced in 4 subsequent aging batches at a temperature of 55 °C and a pH of 6.7 during aging, with a molar ratio of 62.7 % Cu, 29.5 % Zn and 7.8 % Zr (mol %, after calcination) when starting from a mixed metal nitrate solution of the ratio 60:30:10 mol %. Further details on the production and characterization of the CZZ can be found in the ESI (section 1 and Figs. S3–S5). Previous studies have shown that similar continuous co-precipitated CZZ catalysts are highly active in CO_2 hydrogenation, even outperforming the industrial catalyst.[5d,e] For the *operando* experiments in this study, the upper zone was filled with 2 g of undiluted catalyst, whereas the window zone contained 24 mg of diluted (1:5 with SiO_2) catalyst. In this configuration, the window part represents a high conversion zone at the end of a catalyst bed, enabling the study of the impact of a mixture of reactants and products on the catalyst structure. The investigation consisted of an activation step in H_2/N_2, followed by MeOH synthesis and a final step of condensation induced by a temperature drop. Afterwards, a reductive treatment was applied, with the intention to study the degree of catalyst reactivation. The detailed experimental procedures and applied data analyses can be found in the ESI (section 1).

During the initial reaction phase ("reac1"; see ESI, Figure S2), after catalyst activation (spectra during reduction in ESI, section 2.3), CO_2 hydrogenation was operated at 90 bar and 235 °C (T_{sleeve}), and H_2:CO_2 (3:1, 85 % in N_2). This resulted in a CO_2 conversion in the range of 36 to 44 % and a selectivity of 90 % (±2 %) towards methanol during 1.5 h time on stream (TOS) (Figure 2a). The thermodynamic equilibrium at the given conditions was calculated using Aspen Plus. The simulations predict 39 % CO_2 conversion and 90 % selectivity for CO_2 hydrogenation to MeOH, which

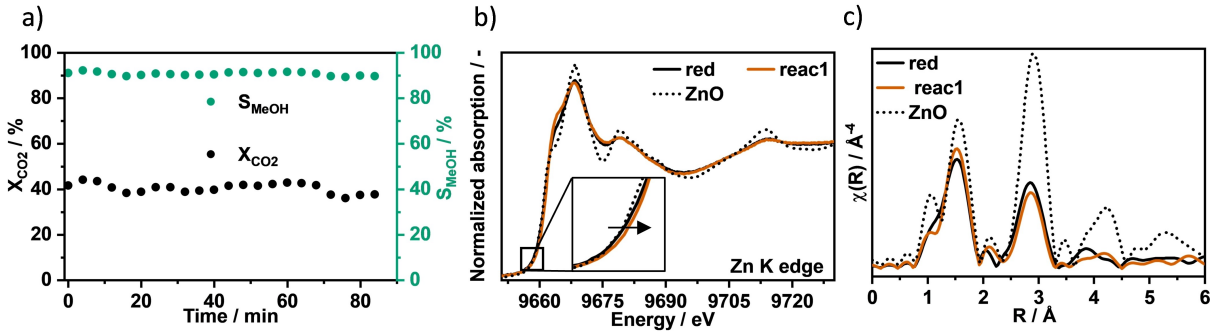

Figure 2. a) CO_2 conversion (black, error estimation ±2%) and MeOH selectivity (green, error estimation ±2%) obtained during CO_2 hydrogenation to MeOH (90 bar, 235 °C, 85% H_2:CO_2 = 3:1 in N_2, reac1, (further details see ESI). XANES (b) and EXAFS (c) spectra at the Zn K edge of the CZZ catalyst after reduction (black line), after CO_2 hydrogenation to MeOH (reac1, orange line) and of the ZnO reference (black dotted line).

agrees with the thermodynamic calculations carried out for this reaction under similar conditions.[25] Comparison with our experimental values clearly shows that the catalyst is operating in equilibrium conditions. Calculating the catalytic performance with Aspen at the same conditions at 10 bar results in 15 % CO_2 conversion and 13 % MeOH selectivity, which further underlines the importance to investigate at high pressure conditions. A slight decrease in CO_2 conversion from 42 % to 38 % was detected throughout 1.5 h TOS. One possible explanation for this behavior is the stabilization period required to reach steady-state conditions and/or slight deactivation of the undiluted catalyst. Structural changes in the upper catalyst bed may be caused by local high temperatures and/or the formation of products passing through the lower section of the bed, potentially leading to further structural changes in the catalyst. The mixture of products and reactants was then passed through the second catalyst bed, which was monitored by XAS (window zone). Throughout this experiment, no differences were observed in spectra recorded in the 3x3 matrix (see additional spectra in Figures S11–S12, ESI). The spectra recorded at the Cu K edge and the corresponding analysis can be found in ESI (sections S2.3 and S2.4). Only small changes in the Cu–Cu scattering shell, possibly indicating slight sintering, were observed during the whole experiment. Given that XAS is a bulk-sensitive method and the catalyst has high Cu loading, these findings only exclude changes in the bulk structure, though minor changes on the surface might not be detectable.

The X-ray absorption near edge structure (XANES) spectra at the Zn K edge of the catalyst, recorded at room temperature after reduction (red., black) and after reaction at 90 bar (reac1, orange), are compared to a bulk ZnO reference (black dotted line) in Figure 2b. Both catalyst states show less pronounced features in comparison to the bulk ZnO reference, indicating a more disordered structure. At the beginning of the absorption edge, a shift to higher energies after reaction was observed (Figure 2b, zoomed in), which can be attributed to an increase in oxidation state. The re-oxidation during reaction under CO_2 hydrogenation conditions was also reported for other Cu–Zn based catalysts.[10a,13,26] Furthermore, the shoulder at 9664 eV emerged under reaction conditions, indicating restructuring of ZnO. Given that this catalyst is exposed to significant concentrations of MeOH and water from conversion in the catalyst bed above, the structural changes are most likely induced by water and/or MeOH. An accelerated formation of a ZnO_x overlayer and restructuring was also found in the presence of MeOH and water for a CZA catalyst.[23] To investigate the local environment, the extended X-ray absorption fine structure (EXAFS) spectra at Zn K edge were extracted (Figure 2c). For both catalyst states, scattering contribution at distances of 1.6 Å (Zn–O, not corrected for the phase shift) and 2.9 Å (Zn-O-Zn) are detected, similar to the ZnO reference. The intensities of the scattering, especially of the Zn-O-Zn contribution, are lower compared to the ZnO bulk reference, which indicates an increased structural disorder in the catalyst. After the reaction, an increase in the first shell (Zn–O) is observed, suggesting further oxygen atoms around Zn in the local structure. This is in line with the energy shift observed in the XANES and the proposed re-oxidation. The second shell backscattering (Zn-O-Zn) decreased after reaction, indicating increased structural disorder, possibly caused by redispersion or restructuring into more amorphous species. A CZZ catalyst investigated at slightly different reaction conditions (H_2/CO_2/CO = 4.3:1:1, p = 60 bar, TOS up to 935 h) showed an increase in the second shell (Zn-O–Zn) suggesting sintering of ZnO.[11d] Hence, the presence of CO seems to affect the catalyst structure additionally. For a Cu-ZnZr catalyst (Cu/Zn/Zr ratio = 2:1:7) prepared by double flame spray pyrolysis (Cu in one flame, Zn + Zr in the other one), a decreased Zn-O-Zn backscattering was observed, similar to our results.[14c] In that case, the decrease in the scattering intensity was attributed to the formation of an amorphous phase or redispersion of Zn. The spraying of the Zn and Zr precursors in one flame led to a strong interaction between ZnO and ZrO_2, even resulting in the formation of monodispersed Zn or ZnO_x clusters.[14c]

To identify the possible Zn species present in our investigation, multivariate curve resolution – alternating least squares (MCR-ALS) analysis was performed on the

entire experimental dataset (details on the procedure see ESI, section 1). The evolution of individual spectral components extracted by MCR-ALS is shown in Figure 3a, and the components with the proposed assignment are displayed in Figure 3b. As seen in Figure 3a, after switching to the reaction conditions (reac1), the component attributed to ZnO (marked in "green", state after reduction) decreased from 100 % to 75 %, while a second component (marked in "pink") increased from 0 % to 25 %. The corresponding spectra (Figure 3b, pink) can be assigned to strongly dispersed (monomeric, dimeric, wurtzite-like structure) ZnO_x species, which are usually observed in combination with zeolites[13] or silicates.[27] So far, analogous ZnO_x species have not been identified for the widely studied CZA catalysts, which might indicate that they only form in the presence of ZrO_2. For systems containing ZrO_2, i.e., mostly as a support, the formation of small ZnO_x clusters or highly dispersed ZnO_x has been reported earlier.[14,28] In comparison to Zn-ZrO_2 compounds with proposed single Zn^{2+} sites,[28–29] our spectra resemble more closely the dimeric ZnO_x species postulated by Zhao and colleagues[27] for a Zn-silicalite catalyst. Additionally, a theoretical XANES calculation of tetrahedral coordinated $[Zn(OH)_4]^{2-}$ species in aqueous solution showed strong similarity with our experimental XANES data.[30] Thus, the hydrogenation of the coordinated oxygen in ZnO to Zn-hydroxyl could yield the dynamic species, which facilitates the dispersion of Zn on the ZrO_2 surface.

ZnO Phase Transformation During Forced Condensation

To investigate the possible catalyst degradation by enforced condensation, the average temperature inside the window zone was lowered down to ~136 °C (T_{window}, reac2), whereas the upper part was continuously heated to 235 °C to produce sufficient MeOH and water. Due to the present temperature gradient (67 °C (T_1) to 206 °C (T_3)), including temperatures above the estimated dew point of 170 °C,[24c] condensation might have only partially occurred or not at all during this state, which explains why no changes were observed during this period. During cool-down to room temperature, and

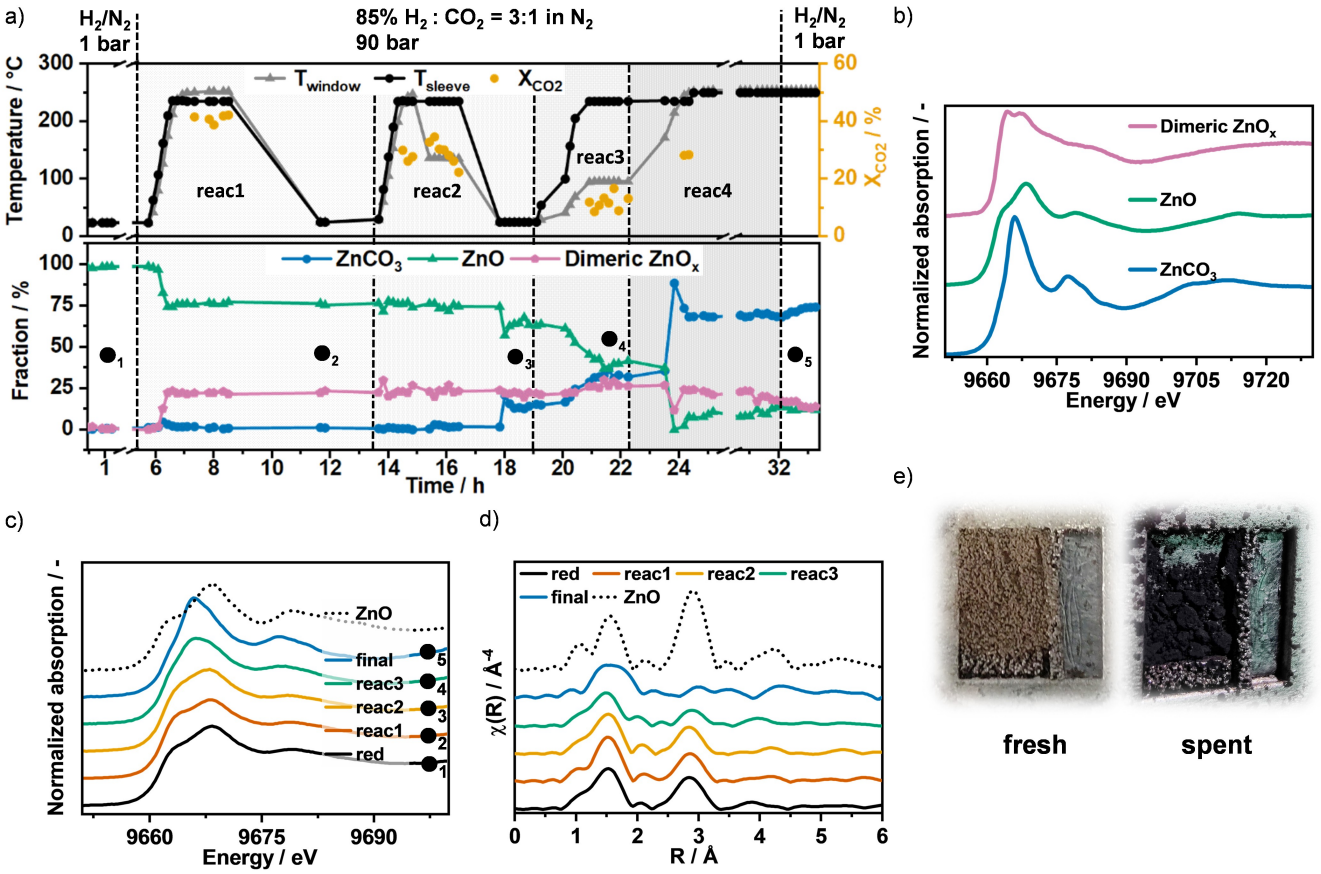

Figure 3. a) Fractions of components obtained by multivariate curve resolution – alternating least square (MCR-ALS) analysis (bottom graph), error estimation ±2 %, recorded temperature of the upper part (T_{sleeve}) and average window zone temperature (T_{window}) (top graph), with the corresponding CO_2 conversions (right y-axis) during the complete experiment (after reduction, reac1-3 and reactivation (reac4), see further details ESI); b) Three obtained Zn K edge XANES of Zn-components from MCR-ALS analysis; c) XANES recorded at the Zn K edge after reduction (red), after various reaction conditions at 90 bar (reac1-reac3), after H_2 treatment (final state) and the ZnO reference; d) EXAFS spectra at the Zn K edge at the same stages as d); e) Photographs of catalyst powder in the X-ray window zone of the reactor as prepared (fresh) and after the experiment with forced condensation (spent).

possibly induced condensation, a third Zn component emerged after 18 h TOS (Figure 3a, blue). The fraction of this species then increased significantly during the cooling of the whole reactor to ambient temperature and continued to increase during the subsequent step (reac3), when the average temperature in the window zone was ~95 °C. The attempt to restart the reaction (reac4) by directly heating the lower part of the reactor again to 235 °C (no depressurization step) led to a further increase of this component. Additionally, a reductive treatment in H_2 did not reverse the induced changes (region 5 in Figure 3a).

In the final state of the experiment, a yet unidentified Zn species was most prominent (Figure 3b, blue, 74 % of all Zn species) while 14 % were present as dimeric ZnO_x (pink) and 12 % as ZnO (green). This change is evident from the experimentally obtained XANES spectra after reactions 1 to 3 and at the final state (Figure 3c), as discussed above. The shoulder at 9664 eV, which emerged during reaction 1, initially increased further during enforced condensation (reac2, yellow, Figure 3c) and then disappeared (reac3 and final state). Simultaneously for reac3 and final state, an increase in the white line intensity and a more pronounced shoulder at 9680 eV were observed (green and blue, Figure 3c). The strong increase in the white line intensity is similar to $[Zn(H_2O)_6]^{2+}$ reported during ZnO nanorod formation from solution under hydrothermal conditions,[31] or Zn-formate, which was postulated as a component of a CZA catalyst present during CO_2 hydrogenation.[10a,13] However, the component detected here exhibits a pronounced shoulder feature at 9680 eV, which is not present in either $[Zn(H_2O)_6]^{2+}$ or Zn-formate, but is characteristic for bulk ZnO or $ZnCO_3$ as observed by comparison with the references.

As in the hydrothermal ZnO rod synthesis reported,[31] a mixture of $[Zn(H_2O)_6]^{2+}$ and ZnO, the latter exhibiting the characteristic shoulder at 9680 eV, could be present. Since Zn formate exhibits almost identical XANES features to $[Zn(H_2O)_6]^{2+}$, we cannot completely exclude that within the isolated Zn component spectrum, a mixture of Zn formate, Zn hydroxyl and bulk ZnO is present. Sintering of ZnO was reported in several long-term deactivation studies.[4a,c,11d,12] According to this hypothesis, strong intensities in Zn-O-Zn shell scattering in EXAFS should be detected. However, the extracted data (Figure 3d) show an overall decrease in the Zn-O-Zn scattering contribution during the condensation period, leading to a final state with barely distinguishable higher shells. Therefore, we exclude the presence of crystalline ZnO. Furthermore, MCR-ALS did not yield meaningful spectral shapes with more than three components, which leads to the conclusion that the third species (Figure 3b, blue) is not a combination of several components.

In a similar ZnO-doped ZrO_2 system investigated by XRD and XAS, the formation of ZnO_x clusters on the ZrO_2 surface was observed, which resulted in an increase in the white line intensity with simultaneous presence of the characteristic shoulder at 9680 eV.[14b] However, the ZrO_2 amount in our sample is much lower (Zn:Zr = 3:1). Furthermore, there is still dimeric ZnO_x present, which can be expected to be localized on the ZrO_2 surface. When comparing the third component (Figure 3b, blue) with $ZnCO_3$ spectra from literature,[32] a similarity in the XANES features and, in addition, with the extracted EXAFS part is found. Similar to Zn formate and $[Zn(H_2O)_6]^{2+}$, $ZnCO_3$ features six octahedrally coordinated O atoms around Zn. Therefore, a geometrical transformation from tetragonal (ZnO) to octahedral ($ZnCO_3$) coordination occurs during condensation, either through highly dispersed Zn species or directly from ZnO. By closely examining the reactivation treatment (reac4, heating under reaction conditions), we first observed a significant increase in $ZnCO_3$, followed by a slight decrease. This indicates that $ZnCO_3$ was formed and thereupon partially decomposed upon further heating. During the increase in $ZnCO_3$, fractions of dimeric ZnO_x species and ZnO decreased, followed by a slight increase. We postulate that $ZnCO_3$ first decomposed to dispersed ZnO_x species, which then agglomerated to ZnO (indicated by the delayed increase of ZnO). At a constant temperature of 250 °C, no further changes were observed, possibly due to a shifted thermodynamic equilibrium at high CO_2 pressures towards carbonate.[33] Therefore, formation of $ZnCO_3$ was likely an irreversible structural alteration at the conditions chosen in this experiment. However, it may be possible to restore the ZnO phase after depressurization and complete drying.

Note that changes were not only observed in the spectra, but also the catalyst bed itself underwent changes in color and texture (Figure 3e). In particular, a change in the catalyst color from brown to black was observed after the testing procedure. Furthermore, the condensation process led to the formation of clumps, thus affecting not only atomic but also the macroscopic properties.

CO_2 conversion as a function of reaction time is plotted in Figure 3a (orange dots). Since the upper zone is filled with 2 g of catalyst and the window zone with only 24 mg of diluted sample, the main conversion stems from the upper zone. A decrease from 40 % CO_2 conversion in the first reaction (reac1) to 30 % in reac2 was observed. As mentioned earlier, initial deactivation due to high temperature and possible condensation in the lower region of the upper reactor part might be the cause. When the temperature in the window zone during reac2 was decreased to 136 °C, a further drop in the CO_2 conversion from 30 % to 22 % was observed. The lower temperature in the window zone might have caused a decrease in the temperature in the lower part of the upper zone, leading to lower activity. Furthermore, back diffusion of condensed products might also contribute to catalyst deactivation in the upper zone. The dimeric ZnO_x (formed during reac1) stayed stable throughout this step (reac2), whereas the ZnO amount slightly decreased, simultaneously with the formation of $ZnCO_3$ species. Such an evolution can be explained by partial transformation of ZnO to $ZnCO_3$. Since the dimeric ZnO_x was not strongly affected under these conditions, it suggests that this configuration is stable, yet possibly not the active species. Decreasing the window zone temperature further to 96 °C (reac3) resulted in further lowering of CO_2 conversion, ranging between 11 and 16 %. As mentioned

above, this might be due to a temperature decrease also in the upper part. With these process parameters, the restructuring to $ZnCO_3$ becomes more pronounced in the window zone. Again, the increase in $ZnCO_3$ was accompanied by a decrease in the ZnO content. In contrast, dimeric ZnO_x showed no changes, which further strengthens the hypothesis that the defective ZnO was transformed into $ZnCO_3$. After heating both the lower and the upper zones of the reactor to 235 °C, conversion to CO_2 was only partially restored, reaching a maximum of 30 %. This shows that irreversible transformations also occur in the upper zone (supported by visual inspection, changed granulate). During heating to 235 °C, the fraction of $ZnCO_3$ drastically increased, with a strong decrease in the ZnO fraction. Increasing the temperature with the condensed products inside the catalyst bed led to distinct hydrothermal conditions, which seem to promote the formation of $ZnCO_3$ from ZnO. Holding the temperature (235 °C) at reaction conditions, with the aim to remove condensed products from the catalyst bed, resulted in a slight decrease of dimeric ZnO_x species and a rise of ZnO. This suggests agglomeration of the dimeric ZnO_x to larger clusters and particles of ZnO or $ZnCO_3$ under these conditions. After depressurization and switching to reductive atmosphere (250 °C, H_2/N_2), a further decrease in dimeric ZnO_x species was observed. However, in this case, also an increase in $ZnCO_3$ was noted, indicating that the dimeric ZnO_x species partially agglomerated with the widely present $ZnCO_3$ species. The selectivity to methanol stayed in the range of 87 % to 91 % during the whole experiment and was not affected by the changes observed in the catalyst structure (details in ESI, section 2.6).

A schematic summary of the proposed Zn components, which are present during reduction, reaction, and forced condensation, is depicted in Figure 4. After activation (Figure 4a), Cu is reduced (see spectra in Figure S7, ESI), whereas ZnO stays mostly oxidized (wurtzite ZnO) while forming some oxygen vacancies or a graphitic overlayer (Figure S8, ESI), similar to the suggestion by Lunkenbein et al.[11a,12] for a CZA and by Warmuth et al.[11d] for a CZZ catalyst. During CO_2 hydrogenation to methanol at 90 bar, when exposed to high product concentrations from the upper zone, the main Zn fraction in the window zone (75 %) stays in the disordered ZnO state, whereas 25 % is present as highly dispersed dimeric ZnO_x (Figure 4b). By comparison with literature regarding similar ZrO_2 containing systems,[14] we postulate that dispersed ZnO_x species are (preferably) stabilized in close contact with ZrO_2. By enforcing condensation inside the window zone of the catalyst bed by lowering the temperature, strong restructuring of Zn occurs leading to formation of a new main component, attributed to $ZnCO_3$, which makes up to 74 % in the final state (Figure 4c). Only 12 % stays as disordered (tetrahedral) ZnO, whereas 14 % of the Zn exist as dimeric ZnO_x species at the end of the experiment. The fraction of dimeric ZnO_x species stayed unchanged during the forced condensation, underlining its stability at those conditions. The formation of $ZnCO_3$ is accompanied by a decrease in ZnO content, which leads to a geometrical change from a tetrahedral coordinated Zn to an octahedral one. This structural change cannot be reversed in the reactor by a temperature increase to 250 °C or under reducing conditions (H_2/N_2) at temperatures that do not lead to strong sintering of Cu. $ZnCO_3$ derived from ZnO could be one pathway to deactivation in the CZZ catalyst. Potentially, a full cycle of unloading, drying, calcination, and subsequent reduction are required to regenerate the catalyst.

In the CO_2-to-MeOH process, similar amounts of water and MeOH are formed concurrently. Therefore, *operando* studies under realistic conditions reveal a combined effect of these two reaction products. Nevertheless, based on literature analysis, the influence of individual liquid products on the catalyst stability can be discussed by considering studies dealing with hydrothermal synthesis of ZnO-based nanostructures in water and alcohol media. Typically, hydrothermal transformations of various Zn precursors (most often, Zn^{2+} salts of inorganic and organic acids) to ZnO nanostructures are performed in water-based media, and solvated Zn-hydroxyl complexes (source of the "dispersed ZnO_x species" XANES spectrum) are deemed to be the mobile intermediate species.[34] However, hydrothermal transformations of Zn species have also been reported in absolute alcohols, albeit with lower

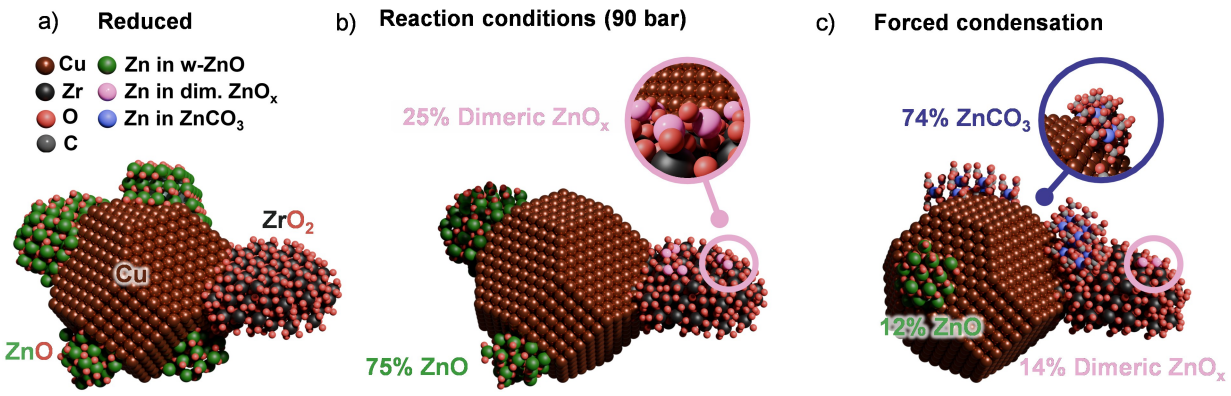

Figure 4. Scheme of present Zn species after a) reduction, b) reaction conditions at 90 bar (reac1) with zoomed-in view of circled area (pink) which shows the dimeric ZnO_x species and c) forced condensation with circled area (pink) to highlight dimeric ZnO_x species and zoomed-in view of the $ZnCO_3$ species (blue).

nucleation and crystal growth rates, resulting in smaller nanoparticles with more defects[35] or even amorphous materials.[36] Hence, while water is probably the main reason for the catalyst deactivation observed in this work, removal of water alone would only slow down but not completely eliminate solvothermal transformations of Zn species. An advanced reactor design which ensures complete separation of the condensed liquid products from the catalyst bed would be required to fully exclude the hydrothermal deactivation described in this work.

Zn spectra obtained at the same conditions (temperature, gas composition) with varying catalyst amount and pressure are compared (Figure S14, ESI) after reduction, reaction conditions and decreased window zone temperature (experimental details in section 1, ESI). With no additional catalyst bed upstream, 8 % CO_2 conversion was achieved, accompanied by only minor differences in the spectra between the three different states. When filling the upper catalyst bed with 1 g of undiluted catalyst and operated at 40 bar, 21 % CO_2 conversion was observed, and changes in the spectra became more pronounced. By further increasing pressure and catalyst amount (this study), we achieved conversions close to equilibrium, leading to significant restructuring of Zn. In Figure 5a these findings are further quantified by linear combination analysis using the spectra obtained from MCR-ALS as references after decreasing the window zone temperature (see details in ESI, section 1), and the corresponding XANES spectra shown in Figure 5b. The fraction of dimeric ZnO_x species (Figure 5a, pink) increases from 6 % to 13 % up to 22 % with increasing CO_2 conversion (recorded before inducing the lower temperature). Simultaneously the fraction of the defective ZnO structure (Figure 5a, green), which was present after reduction, decreases with rising CO_2 consumption, starting from 89 % to 83 %, eventually reaching 65 % in this work. $ZnCO_3$ (Figure 5a, dark blue) increases similar to the dimeric ZnO_x species with 3–5 % below 21 % CO_2 conversion and 14 % in this work as shown above.

This shows that it is important to study catalysts at high conversions, which extends the concept of spatially resolved studies along a catalyst bed[22,37] and offers an alternative to the recently proposed concept proposed by Horn's group on isopotential reactors,[37a] particularly useful for low-pressure reactions.

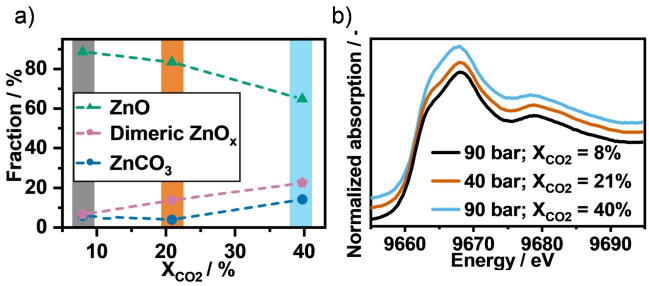

Figure 5. a) Fractions obtained by linear combination analysis plotted against CO_2 conversion obtained at CO_2 methanol synthesis (reac1) at three different experiments: X_{CO2} = 8 %, m_{cat} = 0.03 g, 90 bar, black; X_{CO2} = 21 %, m_{cat} = 1 g, 40 bar, orange; this work: X_{CO2} = 40 %, m_{cat} = 2 g, 90 bar, light blue with the corresponding Zn K XANES spectra shown in (b) obtained after lowering temperature in window zone using a cooling liquid (see further details ESI).

Conclusion

In conclusion, we developed a high-pressure spectroscopic reactor using additive manufacturing, which enabled *operando* XAS studies of a new CZZ catalyst during CO_2 hydrogenation at 90 bar. AM laser metal powder bed fabrication of the catalytic and spectroscopic reactor allowed us to integrate key elements: The X-ray transparent window zone for monitoring the catalyst structure during reaction, and the two consecutive catalyst beds with independently controllable temperatures (heating and cooling). This setup enabled us to study the structure of the catalyst under high conversion, mimicking conditions by catalysts under high stress/conversion, typically observed at the end of a catalyst bed, e. g. when by-products like water are formed. Furthermore, the different temperatures in each of the two catalyst beds enabled investigations under enforced condensation conditions. At elevated pressure (90 bar) methanol synthesis conditions, with a substantial amount of catalyst (2 g) in the upper zone, we achieved an equilibrium CO_2 conversion of 40 %, representing a realistic reaction environment. Under these conditions, we observed the formation of dimeric ZnO_x species, which, by comparison with literature, we concluded to be preferably located on ZrO_2. This species remained mostly stable throughout the experiment, even during forced condensation, indicating that it is not the key interface for catalytic activity. Condensation inside the catalyst bed resulted in irreversible formation of $ZnCO_3$ (reaching almost 75 % in the final state), while the amount of defective ZnO simultaneously decreased (12 % in the final state). In comparison with experiments using lower catalyst amount (without prior catalyst bed) and lower pressures (1 g catalyst, 40 bar), the restructuring of Zn was substantially more pronounced under these equilibrium conditions. Therefore, this study shows the importance of investigating the catalyst structure at relevant and high CO_2 conversion with significant product amounts, especially for the very dynamic Cu–Zn based catalyst system. This emphasizes the need for further investigations in this direction to fully elucidate its structural motif. These studies further complement recent spatially resolved studies in catalytic reactors. In the present setup we can control the conversion in the first catalyst bed by adjusting the catalyst amount and temperature, while monitoring its effect in the second catalyst bed, which is ideal for X-ray spectroscopic probing. Additionally, the proposed deactivation route through $ZnCO_3$ provides a fundamental basis for future catalyst development. Understanding how condensation affects the catalyst structure can guide reactivation treatments aimed at decomposing $ZnCO_3$ without inducing sintering or segregation of the other components. In the future, comparing these findings with those of an industrial catalyst would provide important insights into the role of ZrO_2. Furthermore, the use of additive manufacturing for

designing catalytic spectroscopic reactors demonstrates its potential in advancing our understanding of catalyst dynamics beyond what can be mimicked at low conversion levels. This will also be an important future asset in other reactions, like methanation, ammonia or Fischer–Tropsch synthesis, as well as reforming reactions.

Supporting Information

Additional results and the experimental part can be found in the Supporting Information of this article. The authors have cited additional references within the Supporting Information.[38]

Acknowledgements

We acknowledge Jan Pesek (ITCP), Siegbert Johnson (IKFT) and the KIT workshop for support during construction and installation of the applied experimental setup. For providing helpful feedback during the development of the spectroscopic cell we acknowledge Dr. Marc-André Serrer (ITCP), Uliana Söllner (Siemens), Dr. Robert Otto (Siemens), Dr. Denis Krompass (Siemens) and Dr. Yves Küsters (Siemens). We thank Diana Deutsch (IKFT) for support during the preparation of the catalyst, Thomas Zevaco for performing catalyst characterization measurements, Gabriela Rodrigues Niquini for Aspen calculations and Dr. Karla Herrera-Delgado for fruitful discussions and support in Aspen calculation. We thank Dr. Anna Zimina, Dr. Danielle Santos Goncalves and Markus Makowiak for assistance in beamtime preparation. For graphical assistance, we thank Dr. Florian Maurer. For fruitful discussion on Cu–Zn based catalyst systems and their characterization as well as data visualization, we thank Dr. Arik Beck. We acknowledge the European Synchrotron Radiation Facility (ESRF) for provision of synchrotron radiation facilities under proposal number CH-6776 and we would like to thank Dr. Kirill Lomachenko and Dr. Davide Salusso for assistance and support in using beamline BM23 – XAS Beamline. We further thank the Deutsches Elektronen-Synchrotron (DESY), a member of the Helmholtz Association HGF, for the provision of experimental facilities for beamtime. Parts of this research were carried out at PETRA III at beamline P65 with the proposal number I-20230260 and we would like thank Dr. Edmund Welter, Regina Biller and Marcel Görlitz for the support. We gratefully acknowledge funding of the BMWK Verbundvorhaben 3D-PROCESS (reference numbers 03EN2065B and 03EN2065D) by the German Federal Ministry for Economic Affairs and Climate Action. The authors thank DAPHNE4NFDI (DFG project under project number 460248799) as well as further NFDI-consortia (NFDI4Cat, FAIRMAT and NFDI4Chem) for fruitful discussion and valuable input for implementing FAIR data principles in this work. Open Access funding enabled and organized by Projekt DEAL.

Conflict of Interest

The authors declare no conflict of interest.

Data Availability Statement

After the embargo period the raw XAS data will be available at the ESRF data portal with CC-BY-4.0 licence: Baumgarten, L., Doronkin, D., Schulte, M. L., & Truttmann, V. (under embargo at ESRF until 2026). *Operando* XAS in an additive manufactured reactor with condensation zone during CO2-methanol synthesis [dataset]. European Synchrotron Radiation Facility. 10.15151/ESRF-ES-1357822885.

The data supporting this publication, catalytic activity, temperature and pressure log file and selected XAS spectra are available at KITOpen at https://doi.org/10.35097/ncym5afk9q64kz8x.

Keywords: Heterogeneous catalysis · X-ray absorption spectroscopy · Operando · CO_2-to-methanol · Additive Manufacturing

[1] A. Beck, M. A. Newton, L. G. A. van de Water, J. A. van Bokhoven, *Chem. Rev.* **2024**, *124*, 4543–4678.
[2] a) R. Guil-López, N. Mota, J. Llorente, E. Millán, B. Pawelec, J. L. G. Fierro, R. M. Navarro, *Materials* **2019**, *12*, 3902; b) P. Schwiderowski, H. Ruland, M. Muhler, *Curr. Opin. Green Sustain. Chem.* **2022**, *38*, 100688; c) X. Jiang, X. Nie, X. Guo, C. Song, J. G. Chen, *Chem. Rev.* **2020**, *120*, 7984–8034; d) A. Álvarez, A. Bansode, A. Urakawa, A. V. Bavykina, T. A. Wezendonk, M. Makkee, J. Gascon, F. Kapteijn, *Chem. Rev.* **2017**, *117*, 9804–9838.
[3] V. Dieterich, A. Buttler, A. Hanel, H. Spliethoff, S. Fendt, *Energy Environ. Sci.* **2020**, *13*, 3207–3252.
[4] a) A. Prašnikar, A. Pavlišič, F. Ruiz-Zepeda, J. Kovač, B. Likozar, *Ind. Eng. Chem. Res.* **2019**, *58*, 13021–13029; b) J. Wu, M. Saito, M. Takeuchi, T. Watanabe, *Appl. Catal. A* **2001**, *218*, 235–240; c) B. Liang, J. Ma, X. Su, C. Yang, H. Duan, H. Zhou, S. Deng, L. Li, Y. Huang, *Ind. Eng. Chem. Res.* **2019**, *58*, 9030–9037.
[5] a) F. Arena, K. Barbera, G. Italiano, G. Bonura, L. Spadaro, F. Frusteri, *J. Catal.* **2007**, *249*, 185–194; b) X. Guo, D. Mao, G. Lu, S. Wang, G. Wu, *J. Catal.* **2010**, *271*, 178–185; c) Y. Wang, S. Kattel, W. Gao, K. Li, P. Liu, J. G. Chen, H. Wang, *Nat. Commun.* **2019**, *10*, 1166; d) S. Polierer, D. Guse, S. Wild, K. Herrera Delgado, T. N. Otto, T. A. Zevaco, M. Kind, J. Sauer, F. Studt, S. Pitter, *Catalysts* **2020**, *10*, 816; e) D. Guse, S. Polierer, S. Wild, S. Pitter, M. Kind, *Chem. Ing. Tech.* **2022**, *94*, 314–327.
[6] T. Zou, T. P. Araújo, F. Krumeich, C. Mondelli, J. Pérez-Ramírez, *ACS Sustainable Chem. Eng.* **2022**, *10*, 81–90.
[7] a) F. Arena, G. Italiano, K. Barbera, S. Bordiga, G. Bonura, L. Spadaro, F. Frusteri, *Appl. Catal. A* **2008**, *350*, 16–23; b) F. Arena, G. Mezzatesta, G. Zafarana, G. Trunfio, F. Frusteri, L. Spadaro, *Catal. Today* **2013**, *210*, 39–46.
[8] K. Larmier, W. C. Liao, S. Tada, E. Lam, R. Verel, A. Bansode, A. Urakawa, A. Comas-Vives, C. Copéret, *Angew. Chem. Int. Ed.* **2017**, *56*, 2318–2323.
[9] J. Wang, G. Li, Z. Li, C. Tang, Z. Feng, H. An, H. Liu, T. Liu, C. Li, *Sci. Adv.* **2017**, *3*, e1701290.
[10] a) A. Beck, M. Zabilskiy, M. A. Newton, O. Safonova, M. G. Willinger, J. A. van Bokhoven, *Nat. Catal.* **2021**, *4*, 488–497;

b) J.-D. Grunwaldt, A. M. Molenbroek, N. Y. Topsøe, H. Topsøe, B. S. Clausen, *J. Catal.* **2000**, *194*, 452–460.
[11] a) T. Lunkenbein, J. Schumann, M. Behrens, R. Schlögl, M. G. Willinger, *Angew. Chem. Int. Ed.* **2015**, *54*, 4544–4548; b) M. Behrens, F. Studt, I. Kasatkin, S. Kuhl, M. Havecker, F. Abild-Pedersen, S. Zander, F. Girgsdies, P. Kurr, B. L. Kniep, M. Tovar, R. W. Fischer, J. K. Norskov, R. Schlögl, *Science* **2012**, *336*, 893–897; c) S. Zander, E. L. Kunkes, M. E. Schuster, J. Schumann, G. Weinberg, D. Teschner, N. Jacobsen, R. Schlögl, M. Behrens, *Angew. Chem. Int. Ed.* **2013**, *52*, 6536–6540; d) L. Warmuth, M. Steurer, D. Schild, A. Zimina, J.-D. Grunwaldt, S. Pitter, *ACS Appl. Mater. Interfaces* **2024**, *16*, 8813–8821.
[12] T. Lunkenbein, F. Girgsdies, T. Kandemir, N. Thomas, M. Behrens, R. Schlögl, E. Frei, *Angew. Chem. Int. Ed.* **2016**, *55*, 12708–12712.
[13] M. Zabilskiy, V. L. Sushkevich, D. Palagin, M. A. Newton, F. Krumeich, J. A. van Bokhoven, *Nat. Commun.* **2020**, *11*, 2409.
[14] a) M. T. Nikolajsen, J.-C. Grivel, A. Gaur, L. P. Hansen, L. Baumgarten, N. C. Schjødt, U. V. Mentzel, J.-D. Grunwaldt, J. Sehested, J. M. Christensen, M. Høj, *J. Catal.* **2024**, *431*, 115389; b) D. Salusso, E. Borfecchia, S. Bordiga, *J. Phys. Chem. C.* **2021**, *125*, 22249–22261; c) M. Yang, J. Yu, A. Zimina, B. B. Sarma, L. Pandit, J.-D. Grunwaldt, L. Zhang, H. Xu, J. Sun, *Angew. Chem Int. Ed.*. **2023**, *62*, e202216803; d) X. Zhang, G. Zhang, X. Zhou, Z. Wang, Y. Liu, J. Zhu, C. Song, X. Guo, *Ind. Eng. Chem. Res.* **2023**, *62*, 21173–21181; e) T. Pinheiro Araújo, J. Morales-Vidal, T. Zou, M. Agrachev, S. Verstraeten, P. O. Willi, R. N. Grass, G. Jeschke, S. Mitchell, N. López, J. Pérez-Ramírez, *Adv. Energy Mater.* **2023**, *13*, 2204122; f) X. Zhang, X. Yu, R. G. Mendes, P. Matvija, A. E. M. Melcherts, C. Sun, X. Ye, B. M. Weckhuysen, M. Monai, *Angew. Chem. Int. Ed.* **2025**, 64, e202416899.
[15] T. Pinheiro Araújo, G. Giannakakis, J. Morales-Vidal, M. Agrachev, Z. Ruiz-Bernal, P. Preikschas, T. Zou, F. Krumeich, P. O. Willi, W. J. Stark, R. N. Grass, G. Jeschke, S. Mitchell, N. López, J. Pérez-Ramírez, *Nat. Commun.* **2024**, *15*, 3101.
[16] A. Beck, V. Paunović, J. A. van Bokhoven, *Nat. Catal.* **2023**, *6*, 873–884.
[17] J. Skrzypek, M. Lachowska, M. Grzesik, J. Słoczyński, P. Nowak, *Chem. Eng. J.* **1995**, *58*, 101–108.
[18] L. Pandit, M. A. Serrer, E. Saraçi, A. Boubnov, J.-D. Grunwaldt, *Chem. Methods* **2022**, *2*, e202100078.
[19] N. J. Divins, D. Kordus, J. Timoshenko, I. Sinev, I. Zegkinoglou, A. Bergmann, S. W. Chee, S. Widrinna, O. Karslıoğlu, H. Mistry, M. Lopez Luna, J. Q. Zhong, A. S. Hoffman, A. Boubnov, J. A. Boscoboinik, M. Heggen, R. E. Dunin-Borkowski, S. R. Bare, B. R. Cuenya, *Nat. Commun.* **2021**, *12*, 1435.
[20] A. Bansode, G. Guilera, V. Cuartero, L. Simonelli, M. Avila, A. Urakawa, *Rev. Sci. Instrum.* **2014**, *85*, 084105.
[21] S. Chen, J. Jelic, D. Rein, S. Najafishirtari, F.-P. Schmidt, F. Girgsdies, L. Kang, A. Wandzilak, A. Rabe, D. E. Doronkin, J. Wang, K. Friedel Ortega, S. Debeer, J.-D. Grunwaldt, R. Schlögl, T. Lunkenbein, F. Studt, M. Behrens, *Nat. Commun.* **2024**, *15*, 871.
[22] M. A. Serrer, M. Stehle, M. L. Schulte, H. Besser, W. Pfleging, E. Saraçi, J.-D. Grunwaldt, *ChemCatChem* **2021**, *13*, 3010–3020.
[23] a) D. Li, F. Xu, X. Tang, S. Dai, T. Pu, X. Liu, P. Tian, F. Xuan, Z. Xu, I. E. Wachs, M. Zhu, *Nat. Catal.* **2022**, *5*, 99–108; b) S. Jin, Z. Zhang, D. Li, Y. Wang, C. Lian, M. Zhu, *Angew. Chem.* Int. Ed. **2023**, *62*, e202301563.
[24] a) A. Keshavarz, A. Mirvakili, S. Chahibakhsh, A. Shariati, M. R. Rahimpour, *Chem. Eng. Process.* **2020**, *158*, 108176; b) B. Haut, V. Halloin, H. Ben Amor, *Chem. Eng. Process.* **2004**, *43*, 979–986; c) M. J. Bos, D. W. F. Brilman, *Chem. Eng. J.* **2015**, *278*, 527–532; d) B. Lacerda De Oliveira Campos, K. John, P. Beeskow, K. Herrera Delgado, S. Pitter, N. Dahmen, J. Sauer, *Processes* **2022**, *10*, 1535; e) C. Kiener, (Siemens AG), EP4438206 A1, Germany, **2024**.
[25] K. Stangeland, H. Li, Z. Yu, *Ind. Eng. Chem. Res.* **2018**, *57*, 4081–4094.
[26] E. Frei, A. Gaur, H. Lichtenberg, L. Zwiener, M. Scherzer, F. Girgsdies, T. Lunkenbein, R. Schlögl, *ChemCatChem* **2020**, *12*, 4029–4033.
[27] D. Zhao, X. Tian, D. E. Doronkin, S. Han, V. A. Kondratenko, J.-D. Grunwaldt, A. Perechodjuk, T. H. Vuong, J. Rabeah, R. Eckelt, U. Rodemerck, D. Linke, G. Jiang, H. Jiao, E. V. Kondratenko, *Nature* **2021**, *599*, 234–238.
[28] S. Han, D. Zhao, T. Otroshchenko, H. Lund, U. Bentrup, V. A. Kondratenko, N. Rockstroh, S. Bartling, D. E. Doronkin, J.-D. Grunwaldt, U. Rodemerck, D. Linke, M. Gao, G. Jiang, E. V. Kondratenko, *ACS Catal.* **2020**, *10*, 8933–8949.
[29] D. Zhao, V. A. Kondratenko, D. E. Doronkin, S. Han, J.-D. Grunwaldt, U. Rodemerck, D. Linke, E. V. Kondratenko, *Catal. Today* **2024**, *428*, 114444.
[30] M. Takahashi, H. Tanida, S. Kawauchi, M. Harada, I. Watanabe, *J. Synchrotron Radiat.* **1999**, *6*, 278–280.
[31] K. M. Mcpeak, M. A. Becker, N. G. Britton, H. Majidi, B. A. Bunker, J. B. Baxter, *Chem. Mater.* **2010**, *22*, 6162–6170.
[32] a) M. J. Kwon, M. I. Boyanov, J.-S. Yang, S. Lee, Y. H. Hwang, J. Y. Lee, B. Mishra, K. M. Kemner, *Environ. Pollut.* **2017**, *226*, 346–355; b) T. Luxton, B. Miller, K. Scheckel, in *Speciation Studies in Soil, Sediment and Environmental Samples* (Ed.: S. Bakirdere), CRC Press, Boca Raton, **2013**, pp. 433–477.
[33] S. Kumar, *J. CO2 Util.* **2014**, *8*, 60–66.
[34] S. Baruah, J. Dutta, *Sci. Technol. Adv. Mater.* **2009**, *10*, 013001.
[35] a) K. Nagpal, E. Rauwel, F. Ducroquet, I. Gélard, P. Rauwel, *Nanotechnology* **2023**, *34*, 485602; b) A. Šarić, M. Gotić, G. Štefanić, G. Dražić, *J. Mol. Struct.* **2017**, *1140*, 12–18.
[36] A. M. Ibrahim, M. M. Abd El-Latif, M. S. Gohr, *Egypt. J. Chem.* **2015**, *58*, 475–484.
[37] a) S. Sichert, S.-F. Stahl, O. Korup, R. Horn, *ACS Catal.* **2024**, *14*, 8676–8693; b) J.-D. Grunwaldt, J. B. Wagner, R. E. Dunin-Borkowski, *ChemCatChem* **2013**, *5*, 62–80; c) A. Urakawa, A. Baiker, *Top. Catal.* **2009**, *52*, 1312–1322.
[38] a) S. Brunauer, P. H. Emmett, E. Teller, *J. Am. Chem. Soc.* **1938**, *60*, 309–319; b) M. Thommes, K. Kaneko, A. V. Neimark, J. P. Olivier, F. Rodriguez-Reinoso, J. Rouquerol, K. S. W. Sing, *Pure Appl. Chem.* **2015**, *87*, 1051–1069; c) E. P. Barrett, L. G. Joyner, P. P. Halenda, *J. Am. Chem. Soc.* **1951**, *73*, 373–380; d) O. Hinrichsen, T. Genger, M. Muhler, *Chem. Eng. Technol.* **2000**, *23*, 956–959; e) W. Haiss, N. T. K. Thanh, J. Aveyard, D. G. Fernig, *Anal. Chem.* **2007**, *79*, 4215–4221; f) O. Mathon, A. Beteva, J. Borrel, D. Bugnazet, S. Gatla, R. Hino, I. Kantor, T. Mairs, M. Munoz, S. Pasternak, F. Perrin, S. Pascarelli, *J. Synchrotron Radiat.* **2015**, *22*, 1548–1554; g) E. Welter, R. Chernikov, M. Herrmann, R. Nemausat, *AIP Conf. Proc.* **2019**, *2054*; h) M. Newville, *J. Phys. Conf. Ser.* **2013**, *430*, 0120007; i) G. Landrot, in *Goldschmidt Abstracts*, **2018**; j) B. Ravel, M. Newville, *J. Synchrotron Radiat.* **2005**, *12*, 537–541; k) B. Ravel, *J. Synchrotron Radiat.* **2001**, *8*, 314–316; l) J. Schumann, A. Tarasov, N. Thomas, R. Schlögl, M. Behrens, *Appl. Catal. A* **2016**, *516*, 117–126.

Manuscript received: November 28, 2024
Accepted manuscript online: January 27, 2025
Version of record online: ■■, ■■

Research Article

Operando Spectroscopy

M. L. Schulte, V. Truttmann, D. E. Doronkin, L. Baumgarten, A. Nicolai, D. A. Montalvo Beltran, F. J. Summ, C. Kiener, L. Warmuth, S. Pitter, E. Saraçi, J.-D. Grunwaldt* e202423281

Monitoring the Fate of Zn in the Cu/ZnO/ZrO_2 Catalyst During CO_2-to-Methanol Synthesis at High Conversions by *Operando* Spectroscopy

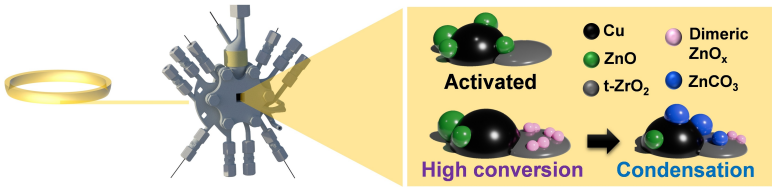

Using an additively manufactured spectroscopic reactor to investigate the structure of a Cu/ZnO/ZrO_2 catalyst with *operando* X-ray absorption spectroscopy during CO_2 hydrogenation to methanol at high conversion. Restructuring of ZnO during high conversion and condensation was observed.